System efficiency analysis of dual interconnected bubbling fluidized bed reactors for solar fuel production

Azharuddin Farooqui, Wladyslaw Jaroszuk, Domenico Ferrero,
Massimo Santarelli and Jordi Llorca

August 29, 2018

System efficiency analysis of dual interconnected bubbling fluidized bed reactors for solar fuel production

Azharuddin E Farooqui[a], Wladyslaw Jaroszuk[b], Domenico Ferrero[c], Massimo Santarelli[d] and Jordi Llorca[e]

[a] *Politecnico di torino, Italy, azharuddin.xxx@polito.it*
[b] *Politecnico di torino, Italy, s238764@studenti.polito.it,*
[c] *Politecnico di torino, Italy, Massimo.santarelli@polito.it*
[d] *Politecnico di torino, Italy, domenico.ferrero@polito.it*
[e] *Universitat Politècnica de Catalunya, Spain, jordi.llorca@upc.edu*

Abstract:

Chemical looping syngas production is a two-step syngas fuel production process that produces CO and H_2. The process is composed of two fluidized bed reactors (oxidation reaction and reduction reactor), oxygen carriers (metal oxides) circulating between the two reactors. A comprehensive model is developed to simulate the chemical looping water and carbon dioxide splitting in a dual fluidized bed reactors interconnected with redox cycling between these two reactors through metal oxides (non-stoichiometric ceria). An extensive FORTRAN subroutine is developed and hooked into Aspen plus V8.8 to appropriately model the complexities of the bubbling fluidized bed reactor including the reaction kinetics. The model developed has been validated for its hydrodynamics and kinetics level and individual correlation was quantified for its validity. The reduction reactor is maintained between the temperatures 1300-1500°C. The heat to attain this high temperature can be achieved with solar beam down tower. The oxidation reactor is supplied with a mixture of CO_2 and H_2O with different mixture composition combining 60% and remaining N_2. The oxidation reactor temperature is varied between 700-1000°C to identify the maximum efficiency achieved. It is found that the maximum efficiency achieved is 67.4% corresponding to highest temperature difference between the reactors.
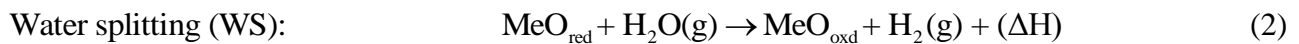
Keywords:

Solar energy, Chemical looping, Solar Fuel, Fluidized beds.

1. Introduction

In the recent years, the direct use of non-fossil fuels synthetically developed starting from CO_2 has been explored as a contribution to the mitigation of fossil carbon emissions. One of the easiest way of dealing the issue is to use carbon dioxide as reactant to prepare hydrocarbons, and to be used in industrial applications [1]–[3]. One of the methods to use carbon dioxide as reactant to produce fuel are thermochemical processes, which harness the solar energy by concentrated solar power systems (CSP) supplying high temperature reactions (usually, chemical loops) that produce synthetic gas. Processes such as steam reforming of methane, coal or biomass gasification, water splitting (WS) to hydrogen, splitting of carbon dioxide (CDS) to form CO which is one of a constituent of syngas require high temperature of operation. Among the existing thermochemical routes reforming is considered to be performed at low temperatures compare to WS and CDS process [4].

Number of thermochemical cycles has been proposed with multiple steps: among those, two-step based on oxide redox pair systems has shown great potential for synthetic solar fuel generation. These thermochemical cycles operate on the principle of transition between higher valence oxidized (MeO_{oxd}) and lower valence reduced (MeO_{red}) form of an oxide of a metal having multiple oxidation states [5]. The first higher temperature endothermic step requires higher valence oxide of

a metal that is undergoes a thermal reduction (TR), i.e., release of oxygen upon supply of external heat to form a lower valence oxide of metal. In the second step, the reduced metal oxide is oxidized back to higher valence state by taking oxygen from water and/or CO_2, then resulting in H_2 and CO in WS and CDS reaction respectively. Here, Tred>Toxd is the thermodynamic demand for this process to be attainable [6]. However the partial pressure change during the oxidation and reduction affects the process drastically, and especially the reaction kinetics would play a role in defining the overall efficiency of the process.

Thermal reduction (TR): $$MeO_{oxd} + (\Delta H) \rightarrow MeO_{red} + 0.5O_2(g) \qquad (1)$$

Water splitting (WS): $$MeO_{red} + H_2O(g) \rightarrow MeO_{oxd} + H_2(g) + (\Delta H) \qquad (2)$$

Carbon dioxide splitting (CDS): $$MeO_{red} + CO_2(g) \rightarrow MeO_{oxd} + CO(g) + (\Delta H) \qquad (3)$$

The temperature and valence shift within the reaction is shown by a general schematic in figure 1:
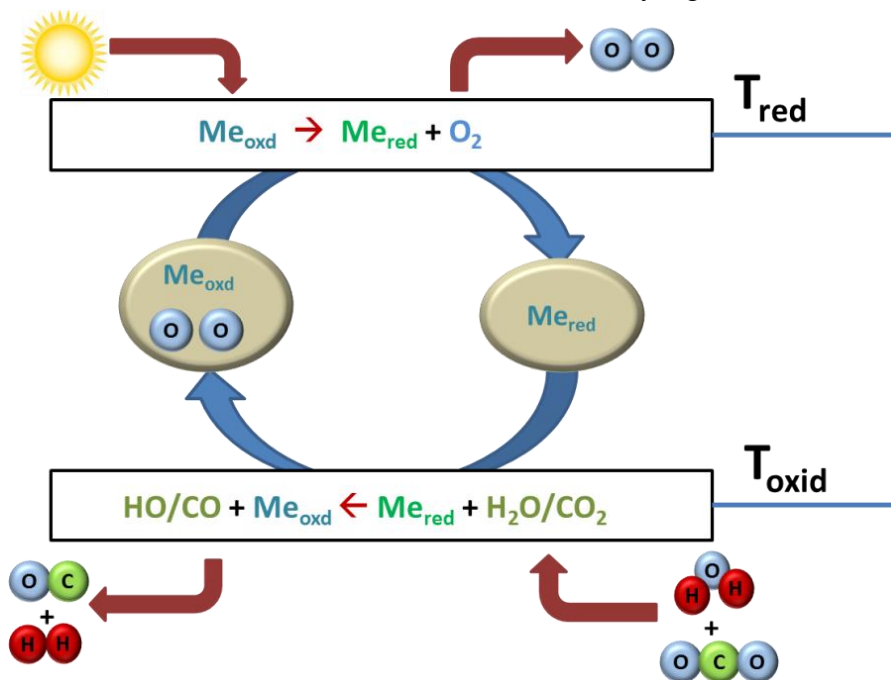

Fig. 1 Schematic of two-step thermochemical redox cycle

The oxygen production during the first step depends on the reduction extent and the metal cation of highest valence that is reduced. Highest possible dissociations are in principle sought, the higher the oxygen released during dissociation the higher the oxygen taken from H_2O and CO_2 during oxidation, resulting in higher H_2 and CO production per mass of redox material and thus higher efficiency [6]–[10]. The cycle efficiency is also defined as the higher heating value of the fuel produced to the thermochemical cycle energy input. Some pairs are composed by metal oxide/metal systems (such as ZnO/Z; SnO/Sn) or metal oxide/metal oxide systems (Fe_3O_4/FeO; Mn_3O_4/MnO; CeO_2/Ce_2O_3, etc) [10]. Other metals oxides tested are ferrites with different valences, Co_3O_4, Nb_2O_5, WO_3, SiO_2, In_2O_3, CdO to name few [11]–[15].

CeO_2 is largely investigated in literature for its structural, chemical and optical properties that make it a promising material in several fields of applications, such as fuel cells, catalysis, CO_2 adsorbing materials, nanofluids etc [16]. Furthermore, it is also demonstrated that the CeO_2 preserves its optical properties, even after several runs of thermal processes. It also shows very minimal effect of sintering at high temperature with good attrition resistance and mechanical strength that makes it a good candidate to investigate and use for large scale units for CO_2/H_2O splitting application [17].

Furler et al. [18] investigated high flux solar simulator to study the feasibility of CeO_2 based cavity reactor. The study reported that the solar-to-fuel energy conversion efficiency which was defined as calorific value of fuel produced to solar radiative energy through the reactor aperture and energy penalty for using sweep inert gas was 1.73% with peak achieved as 3.53%. In order to improve the system with respect to the scale and efficiency, a moving packed bed of reactive particle reactors have been employed to investigate and analyse the efficiency [19]. The packed bed reactor combines several features, essential to achieve high efficiency: spatial separation of pressures, temperature and reaction products in the reactor, and solid-solid sensible heat recovery between reaction steps, continuous on-sun operation and direct solar illumination of the working material. They show that in a fully developed regime, using CeO_2 as a reactive material, the conversion efficiency of solar energy into H_2 and CO at the design point can exceed 30%. The packed bed operation limits the volume of the syngas production due to its limitation of lower gas inflows and size of the reactor.

In the present work, a new model of solar reactor, based on a double-loop fluidized bed, involving CeO_2 is presented. The model presented in the study is developed considering the two fluidized bed interconnected with CeO_2 circulating between them. The fluidized beds were considered to be operating in bubbling mode regime. The effect of temperature of the reactors and its effect on efficiency have been investigated.

2. Model description

The model developed deals with two fluidized bed reactors in bubbling mode interconnected with metal oxide circulating between them. Each fluidized bed model developed considers two different zones: the bottom zone, also called as Dense Phase (DP) characterized by high solids volume concentrations, and the upper dilute zone or Freeboard (FB) in which the solids volume concentration decreases with increasing height. The bottom zone is modeled as a bubbling bed according to Werther & Wein [20] and the upper dilute zone follows the approach according to Kunnii & Levenspiel [21]. The void space within the bed can be characterized as having two distinct phases: the bubble and the emulsion. These fluid dynamic models were used with other correlations to describe the distribution of solids along the fluid bed, and for entrainment considerations.

2.1 Hydrodynamics

There are a couple of phenomena occurring in the dense phase of the reactor that describe the hydrodynamics in this phase. Arguably the most important set of parameters describing how the bed operates is the minimum fluidization properties—velocity (u_{mf}) and voidage (ε_{mf}). These two properties of the fluidized bed, or more rather particles within it, are used during the whole process of modelling to calculate everything from actual bed voidage (ε_{mf}) to bubble rise velocity (u_b).

██████ Minimum fluidization voidage and minimum fluidization velocity

The parameters have been calculated based on the equations presented by [21] in table 1.

Table 1. Hydrodynamics parameters used in the fluidized bed model

Reynolds number of the particle	$\mathrm{Re}_p = \sqrt{33.7^2 + 0.04084 Ar_p} - 33.7$
Reynolds number and Archimedes number for minimum fluidization velocity	$\mathrm{Re}_p = u_{mf} \cdot \rho \cdot d_p / \mu_g$; $Ar_p = d_p^3 \cdot \rho_g \cdot (\rho_s - \rho_g) \cdot g / \mu_g^2$
Maximum bubble volume before it detaches orifice surface as	$V_{bo} = 1.138 v_{or}^{1.2} / g^{0.6}$
Initial bubble diameter	$d_{bo} = 1.3 \left((u_o - u_{mf}) / N_{or} \right)^{0.4} / g^{0.2}$; N_{or} is the number of orifices.
Maximum bubble diameter	$d_b(h) = d_{bm} - (d_{bm} - d_{b0}) \exp(-0.3 h / d_t)$ where $d_{bm} = 0.649 \left(A_t \left(u_o - u_{mf} \right) \right)^2$
Bubble absolute rise velocity: general form	$u_b = u_0 - u_{mf} + u_{br}$
bubble rise velocity	$u_{br} = 0.711 \sqrt{g d_b}$
absolute bubble rise velocity	$u_b = 1.55 \cdot \left\{ (u_0 - u_{mf}) + 14.1 \cdot (d_b + 0.005) \right\} d_t^{0.32} + u_{br}$
overall voidage of the bed	$\varepsilon_f = \delta + (1 - \delta) \varepsilon_e$
Solids volume fraction	$\varepsilon_s = 1 - \varepsilon_f$
bubble volume fraction	$\delta = (u_0 - u_{mf}) / (u_b + 2 \cdot u_{mf})$
Emulsion velocity	$u_e = u_{mf} / \varepsilon_{mf}$
Emulsion voidage ε_e	$\left(\varepsilon_e / \varepsilon_{mf} \right)^3 \left((1 - \varepsilon_{mf}) / (1 - \varepsilon_e) \right) = \left(u_e / u_{mf} \right)^{0.7}$

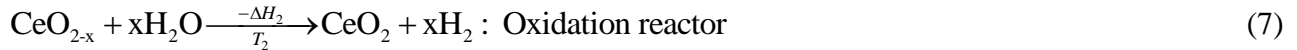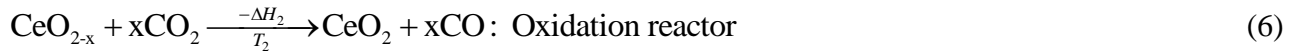## ███ Elutriation of particles from the fluid bed

As the gas travels through the dense phase of the bed, bubbles grow and finally reach the border of the dense phase zone. Kunii and Levenspiel [21] described mechanism which leads to ejection of solid particles from the dense phase. Proposed behaviour of the phenomenon is connected to bubbles bursting as they reach surface of the dense phase and subsequent transport of the lump of solids travelling in the bubble wake into the freeboard due to its inertia. Another source of solids material in the freeboard was observed by Rowe and Partridge [22]. They have noticed that significant portion of solids did not come from the bubble wake, but from the particles present in front of the bubble when it burst. There is little amount of data allowing to assess the entrainment rate at the dense zone's surface given the complexity of the process and lack of common agreement on which is the dominating process. In general, in models presented in literature [23], [24] approach based on "projection" of solids volume fraction from the dense zone is used. This method, in a way, assumes that there is no distinguishable limit between the dense phase and the freeboard zone, which is true in the turbulent and fast fluidizing beds.

This approach might not be necessarily true especially in case of slow bubbling beds, where bursting bubbles have insufficient energies to carry that amount of solids into the freeboard. Wen and Chen [25] presented a different approach and the correlation between entrainment rate from the bed and bubble diameter as well as excess gas flow term was developed and is presented in eq (4).

$$F_0 = 3.07\varepsilon - 9\frac{\rho_g^{3.5} g^{0.5}}{\mu_g^{2.5}}\left(u_0 - u_{mf}\right)^{2.5} \cdot A_t d_b \tag{4}$$
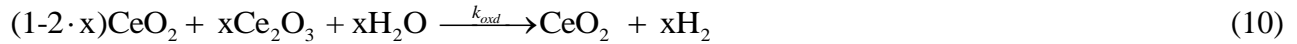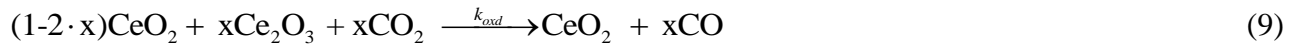
2.2 Reaction kinetics

With progress of research in exploring new materials, most of the work is now focused on non-stoichiometric materials such as Ceria that showed higher oxygen storage capacity and able to operate at lower reduction temperature. In reduction reactor, ceria releases oxygen and undergoes thermal reduction while in oxidation reactor the reduced ceria undergoes oxidation with incoming carbon dioxide and water producing carbon monoxide and hydrogen. The reactions of ceria undergoing in both reactors are presented below:

$$CeO_2 \xrightarrow[T_1]{\Delta H_1} CeO_{2-x} + \frac{x}{2}O_2 \; : \; \text{Reduction reactor} \tag{5}$$

$$CeO_{2-x} + xCO_2 \xrightarrow[T_2]{-\Delta H_2} CeO_2 + xCO : \; \text{Oxidation reactor} \tag{6}$$

$$CeO_{2-x} + xH_2O \xrightarrow[T_2]{-\Delta H_2} CeO_2 + xH_2 : \; \text{Oxidation reactor} \tag{7}$$

All of these reactions are heterogeneous and non–catalytic. Aside from the fact that reduction and oxidation occur in different temperatures, they have also different energy effect. Ceria reduction reaction (5) is endothermic while oxidation reactions (6) and (7) are exothermic.

The reactions (8), (9) and (10) are based on the non-stoichiometric ceria. Since there are no thermodynamic properties of non-stoichiometric ceria available in literature, a different approach has been used. The reduction reaction is modelled as equation (8). Here non–stoichiometry factor x is used to define ratio between still unreacted ceria and reduced form–Ce_2O_3. Later mixture can be used in the oxidation reaction such as equation (9) and (10).

$$CeO_2 \xrightarrow{k_{red}} (1\text{-}2\cdot x)CeO_2 + xCe_2O_3 + 0.5xO_2 \tag{8}$$

$$(1\text{-}2\cdot x)CeO_2 + xCe_2O_3 + xCO_2 \xrightarrow{k_{oxd}} CeO_2 + xCO \tag{9}$$

$$(1\text{-}2\cdot x)CeO_2 + xCe_2O_3 + xH_2O \xrightarrow{k_{oxd}} CeO_2 + xH_2 \tag{10}$$

In the kinetics model developed, degree of advancement of reaction is used instead of non-stoichiometry coefficient due to limitations explained earlier. This definition would require calculation of separate α parameters for all of the reactions. It is noticed though, that degree of advancement of the reaction can be calculated in terms of Ce_2O_3 content. It is represented by equation (11)

$$\alpha = \frac{\dot{n}_{Ce_2O_3}}{\dot{n}_{Ce_2O_3} + 0.5 \cdot \dot{n}_{CeO_2}} \tag{11}$$

$$\dot{n}_{Ce_2O_3} + 0.5 \cdot \dot{n}_{CeO_2} = \dot{n}_{OC} \tag{12}$$

The equation (12) describes degree of reduction of ceria powder. Numerator contains information about current content of Ce_2O_3 and denominator about maximum possible content of this species. Thus denominator of this equation is always constant and represents molar flow of fully reduced oxygen carrier (equation 12). More information on calculation of degree of advancement of reaction is explained in the following subsections. Such formulation of degree of advancement of thermal reduction reaction ($\propto_{red}$) suits reduction kinetic model developed by Ishida et al [26]. Non-stoichiometric coefficient is given as equation (13).

$$x=0.5\alpha_{red} \tag{13}$$

Reduction kinetics

The thermal reduction kinetics are reported to be slow as the reaction is mainly depended on the temperature only. Ishida et al [26] investigated ceria reduction considering N_2 as sweep. Different reaction models were correlated with the experimental data; the most fitting were reaction order–based models F1-F3. From those, first order based model fitted overall data best, and thus the following rate equation (14) was proposed.

$$\frac{d\alpha_{red}}{dt} = A_{red} \cdot \exp\left(-\frac{E_{red}}{RT}\right)(1-\alpha_{red}) \tag{14}$$

$$\alpha(\tau) = \left(\int_{t=0}^{t=\tau} n_i dt\right)/n_{itot} \tag{15}$$

Where α_{red} is the degree of advancement and value of the parameters are given in table 2. R is the universal gas constant (kJ/mol-K) and E_{red} is the reduction activation energy, n_i is the current quantity of the reactant i, mol; n_{itot} is the total quantity of the reactant, if the reaction reached equilibrium state, mol

Table 2: Ceria reduction rate equation coefficients presented by Ishidi et al [26]

Parameter	Value
A_{red} (1/s)	175.1
E_{red}, kJ/mol	172.1

Having defined derivative of degree of advancement of the reaction with respect to time as equation (14), transition from this to reaction rates of the concerned species is done the following way by equation (16).

$$\frac{d\alpha_{red}}{dt} = \frac{d}{dt}\left(\frac{\dot{n}_{Ce_2O_3}}{\dot{n}_{Ce_2O_3} + 0.5\dot{n}_{CeO_2}}\right) = \frac{d}{dt}\left(\frac{\dot{n}_{Ce_2O_3}}{\dot{n}_{OC}}\right) = \frac{1}{\dot{n}_{OC}}\left(\frac{d\dot{n}_{Ce_2O_3}}{dt}\right) \tag{16}$$

Equation (16) combined with reduction model gives time derivative of the Ce_2O_3 molar flow rate. This reaction has three species taking part in it, for each cerium oxide mole created two moles of ceria are consumed and half of mole of oxygen gets released. Aside from stoichiometric coefficients, knowledge of reaction time step is needed. In this discrete model particle residence time is used as the time parameter. The thermal reduction reaction rates are presented as the following equation (17), (18) and (19).

$$k_{redCeO_2} = -2 \cdot \dot{n}_{OC} \frac{d\alpha_{red}}{dt} \Delta t \tag{17}$$

$$k_{redCe_2O_3} = 1 \cdot \dot{n}_{OC} \frac{d\alpha_{red}}{dt} \Delta t \tag{18}$$

$$k_{redO_2} = 0.5 \cdot \dot{n}_{OC} \frac{d\alpha_{red}}{dt} \Delta t \tag{19}$$

Oxidation kinetics

The oxidation kinetics for the ceria was adopted from [27]. The kinetic data reported is obtained for thermally reduced ceria and oxidized by H_2O and CO_2 in the temperature range of 750-950°C for water vapour and 650-875°C for carbon dioxide and volume fraction of H_2O was varied from 20-40% and CO_2 between 10-40%. The reaction mechanism has been proposed in the general formulation for the reaction rate as equation (20) and coefficients are listed in table 3.

$$\frac{d\alpha_{oxd}}{dt} = A_0 \cdot \exp\left(-\frac{E_0}{RT}\right) y_i^{\gamma} (1-\alpha_{oxd})^n \tag{20}$$

Where α_{oxd} is the degree of the advancement of the reaction, E_0 is the oxidation activation energy, y_i is the oxidant molar fraction.

Table 3: Kinetic parameters of the oxidation reaction of reduced ceria obtained by Arifin [27]

Oxidant	Temp (^{o}C)	A_0 (1/s)	E_0 (KJ/mol)	γ (-)	n(-)
CO_2	750-950	1.0	29	0.89	1.0
	650-725	4.2	47	0.53	1.0
H_2O	750-800	3.4	45	0.65	1.2
	825-875	2.5	41	0.7	1.7

It is stated that reaction of oxidation with water vapor is behaving similarly to homogeneous reactions, i.e. its rate decelerates proportionally to the depletion of the reactants ($1-\alpha_{oxd}$). More so, water splitting has relatively small activation energy of 29 kJ/mol, which helps its kinetics greatly. The same analysis reported for carbon dioxide splitting revealed dependence of the rate-determining step on the temperature of the process. It also indicates that as temperature increases carbon site blocking and subsequent surface recombination stops, at 875°C only reaction pathway is direct desorption of carbon monoxide from the particle surface. These phenomena cause change in the coefficients γ and n (in table. 3). It is worth noticing here, in discussed research ceria sample was constantly cycled and reused in different conditions, nevertheless Arifin [27] noted that overall production of the fuel from the sample remained almost constant, though reaction times varied because of varying temperatures and molar fractions of reactants.

For determination of reaction rates, the degree of advancement of oxidation reaction is calculated as equation (21).

$$\alpha_{oxd} = 1 - \alpha_{red} \tag{21}$$

Independently of the selected oxidants CO_2 and H_2O, when one mole of each is consumed it leads to simultaneous consumption of each mole of Ce_2O_3. As an effect two moles of Ceria and one mole of CO and H_2 is created. Taking this into account, the reaction rates for each species are listed as:

$$k_{oxdCeO_2} = 2 \cdot \dot{n}_{OC} \left\{ \frac{d\alpha_{oxdH_2O}}{dt} + \frac{d\alpha_{oxdCO_2}}{dt} \right\} \Delta t \tag{22}$$

$$k_{oxdCe_2O_3} = -1 \cdot \dot{n}_{OC} \left\{ \frac{d\alpha_{oxdH_2O}}{dt} + \frac{d\alpha_{oxdCO_2}}{dt} \right\} \Delta t \tag{23}$$

$$k_{oxdH_2O} = -1 \cdot \dot{n}_{OC} \frac{d\alpha_{oxdH_2O}}{dt} \Delta t \tag{24}$$

$$k_{oxdH_2} = 1 \cdot \dot{n}_{OC} \frac{d\alpha_{oxdH_2O}}{dt} \Delta t \tag{25}$$

$$k_{oxdCO_2} = -1 \cdot \dot{n}_{OC} \frac{d\alpha_{oxdCO_2}}{dt} \Delta t \tag{26}$$

$$k_{oxdCO} = 1 \cdot \dot{n}_{OC} \frac{d\alpha_{oxdCO_2}}{dt} \Delta t \tag{27}$$

2.3 Validation

Overall hydrodynamics model has been tested against experimental data provided by Taghipour et al. [28]. The experimental results were obtained on rectangular bed, this amplifies wall effects on the experiment and thus results are different from what could be expected in the cylindrical set–up. Neither specific distributor configuration nor pressure drop was reported, thus their values have had to be assumed in the run. Validation has been done for the bed filled with spherical glass beads of density of 2500 kg/m^3. Average particle diameter was 275 μm. Experimental set–up bed dimensions were 0.28m of width, 0.0025m of thickness, 1m of height. Modelled reactor dimensions were set to 0.28m of diameter and 1m of height. Distributor pressure drop of $0.3\Delta p_b$ was assumed. Inlet gas pressure was calculated to be higher than atmospheric by this value; in this situation dense phase inlet pressure is equal to atmospheric. Mass holdup was calculated based on the data provided by Taghipour et al [28]—static bed height of 0.4m and static solids volume fraction of 0.6. Based on the data and on the reactor dimensions solids holdup is calculated as approximately 37 kg. Model agreement with the experimental data was checked in 5 different inlet superficial gas velocities: 0.1; 0.2; 0.3; 0.4; 0.5 m/s. Three parameters have been compared between simulation and the experimental data. In the experiment bed pressure drop increased from 4.5 to 5.75 kPa as the superficial velocity increased, in the model this parameter is constant and equal to 5.9 kPa. Result is slightly overestimated mainly due to the difference in bed geometries and difficulty in predicting actual mass holdup in the bed. In addition, experimental pressure drop is calculated only up to 0.6m of the bed height, while the modelled drop is across whole reactor.
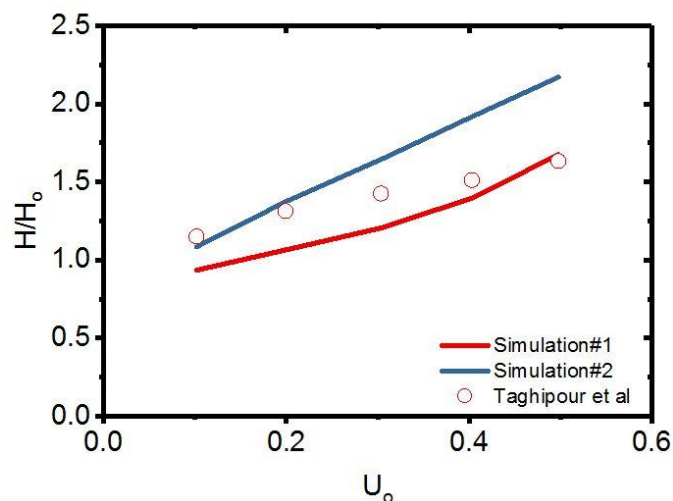

Fig. 2. Comparison of the bed expansion coefficients obtained from the simulation and experiment. #1 was obtained in the F_0 projection model set–up, #2 Wen and Chen correlation F_0 model set–up.

From the figure 2, it is shown that hydrodynamic bed model follows the behavior closely. It is noted that for slow fluidizing beds in the area of minimum fluidization and minimum bubbling conditions Wen and Chen model predicts bed behaviour much better—relative error of approx. 5%. In the faster fluidizing regimes and vigorously bubbling beds projection of entrainment rate from the dense phase surface fits experimental data more closely—relative error of approx. 7%. One of the reasons for such behaviour might be the fact that in the slow fluidizing beds predominant particles entrainment mechanism is bursting of bubbles represented in Wen and Chen model. As the fluidization speed increases gases have more energy and start entraining particles also from the dense phase. From these observations it is suggested to consider Wen and Chen's entrainment model whenever superficial velocity is lower than $6u_{mf}$, above this value the second discussed model gives more accurate results. The difference in the fluid bed layouts is considered the main reason for the discrepancies in between experimental data and the simulation. In the rectangular

beds wall effects have significant influence on the particles movement and on the obtained results. Bubbles rising in those types of beds are always slugs in one dimension, which influences calculation of parameters such as voidage and subsequently bed expansion.

3. Model set-up and system analysis

In the system design and optimization, the important factors are the amount of bed material in the two reactors that must be adequate for a sufficient conversion of reacting gas, and the circulation rate between the reactors that must be high enough to transport the oxygen carriers to take away the oxygen from the reacting gases and produce synthetic fuel; the third is the gas leakage between the reactors that must be minimized. The first two are dependent on the characteristics of the oxygen carrier used, as solid reactivity, type of metal oxide. In order to design the system, the reduction reactor is firstly designed, and then the oxidation reactor as its size directly depends on the inlet solids composition i.e., reduction process performance. The system layout was created with user blocks in AspenPlus V8.8 and the hydrodynamics and kinetics are written in FORTRAN and linked with AspenPlus. For thermophsyical properties, UNIFAC calculation method is adopted. The description of the system layout is presented in figure 3.
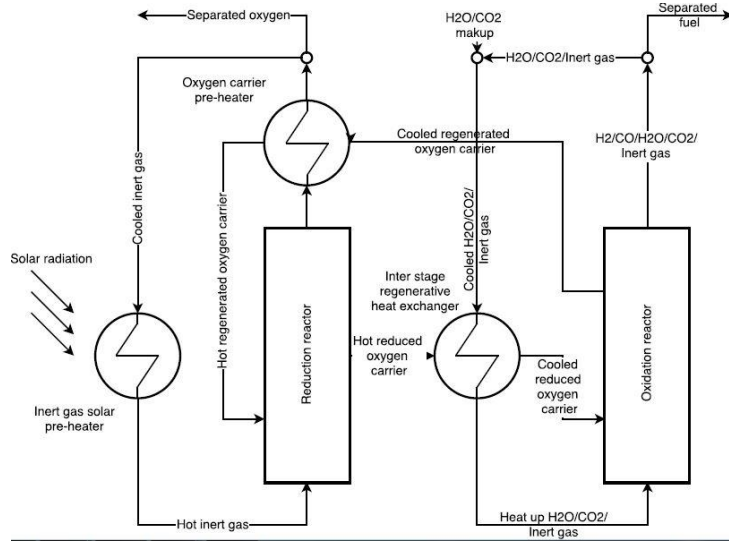

Fig. 3. System layout of the interconnected fluidized bed

4. Results

The reduction reactor considered has oxygen carriers with average particle diameter of 100 μm and sphericity of $\phi_s = 1$. The reduction reactor has 1 m of diameter and 3 m of height. Orifice distributor is selected with pressure drop considered as $0.4\Delta p_b$. The gas distributor has orifices in triangular configuration with spacing of $l_{or}=0.03$m and number of orifice considered are $n_{or}=1008$. Minimum fluidization velocity was determined by Ergun equation, solids entrainment at the bed surface projected model was selected and Elutriation rate constant is calculated based on Wen and Chen model. Both dense and freeboard zone were divided into 100 elements and particles were divided into 100 size classes of Geldart B classification. The reactor is modelled as isothermal but the reaction in the reactor is endothermic. Thus, to keep the temperature constant certain amount of heat has to be delivered. The heat required in the reduction reactor is determined by equation (28).

$$\dot{Q}_{red} = \dot{m}_{gin}\dot{h}_{gin} + \dot{m}_{sin}\dot{h}_{sin} - \dot{m}_{gout}\dot{h}_{gout} - \dot{m}_{sout}\dot{h}_{sout} \qquad (28)$$

Where 'gin' denotes the inlet gas stream, 'sin' is the inlet solids stream, 'gout' is the outlet gas stream and 'sout' is the outlet solids stream. The make-up solid inlet stream of 5 kg/s of Ceria is considered.

The inlet gas sweep gas stream for reduction reactor was considered as N_2. The temperature in the reactor is varied from 1300-1600°C range. The lower limit has been determined as the point in which the reduction reaction starts to be noticeable by releasing oxygen, though it occurs also in lower temperatures but with very low reduction rates. The upper limit of the temperature is chosen such that to avoid the significant sintering of the particles in the bed, though from the kinetics the higher the temperature the more the oxygen release. The velocity of inlet sweep Nitrogen was 0.05 m^3/s and solid inventory of the reduction reactor assumed as 3600 kg. The oxidation reactor was set to 2 m diameter and 2 m height with a solid inventory of 6000 kg fixed. The temperature of oxidation reactor is varied from 700-1000°C. The inlet gas flow and its composition ($H_2O:CO_2:4:1$) were 60% with remaining N_2 in order to assess performance to access the H_2/CO ratio at the exhaust.

It can be seen from the figure 4, with the increase of the reduction temperature, the oxygen production at the exit of reduction reactor increases. This is due to non-stoichiometric ceria is releasing oxygen and oxygen vacancies are created before it is being transported to the oxidation reactor. It is observed that the O_2 release reaches the maximum value of 0.001 kmol/s for the reduction temperature of 1550 ^{o}C. The influence of oxygen release in the reduction reactor has very little influence of oxidation reactor temperature.
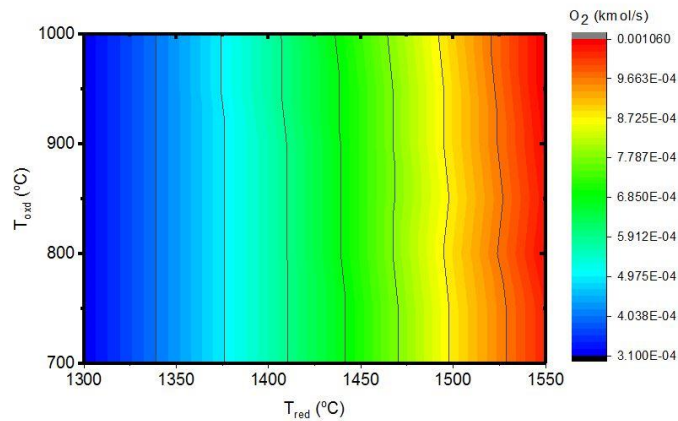

Fig. 4. Oxygen output at the exit of the reduction reactor for various oxidation and reduction temperatures
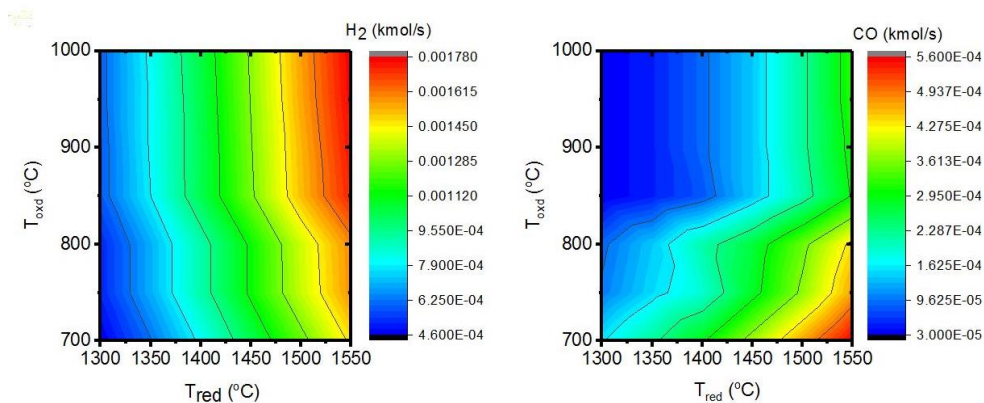

Fig. 5. H$_2$ and CO production at the exit of the oxidation reactor for varying oxidation and reduction temperatures.

From Figure 5 it is seen that the H_2 production and CO production both increases with increase of reduction temperatures with the maximum H_2 as 0.00178 kmol/s and CO as 5.6e-04 kmol/s. The result shows that the profiles of production of both the species are different and leading to higher and higher H_2/CO ratio with increase of difference of temperatures between the reactors. It also signifies the kinetics of H_2 is fast and favourable at higher temperature of oxidation reactor for a particular reduction temperature, whereas for CO it is seen that the reaction is favourable at lower temperature but it follows the slow kinetics making the H_2/CO ratio higher. In order to have appreciable H_2/CO ratio it would be wise to operate the oxidation reactor around 700-800°C and reduction reactor between 1400-1500°C.

Energy efficiency of the process can be calculated assuming that both reduction reactor and solids released from the oxidation reactor are preheated with solar source, with efficiency $\eta_s = 0.85$. Equation (29) is system efficiency considering the pre-heating of the solids, gas reactants in both the reactor and heat recuperated from solids.

$$\eta_{\text{sysII}} = \frac{\dot{m}_{H_2} LHV_{H_2} + \dot{m}_{CO} LHV_{CO} + \dot{Q}_{\text{oxd}} + \dot{Q}_{\text{scld}}}{\frac{1}{\eta_s}(\dot{Q}_{\text{red}} + \dot{Q}_{\text{spht}} + \dot{Q}_{\text{loss}})} \qquad (29)$$

Where $\dot{Q}_{\text{loss}} = 0.1 \cdot (\dot{Q}_{\text{red}} + \dot{Q}_{\text{spht}})$ and $\dot{Q}_{\text{scld}}$ is the heat recovered from solids from reduction reactor before it enters oxidation reactor, $\dot{Q}_{\text{oxd}}$ heat recovered from the oxidation reactor, $\dot{Q}_{\text{red}}$ heat recovered from the reduction reactor, $\dot{Q}_{\text{spht}}$ heat delivered to solids for preheating, $\dot{Q}_{\text{loss}}$ heat loss in the system.
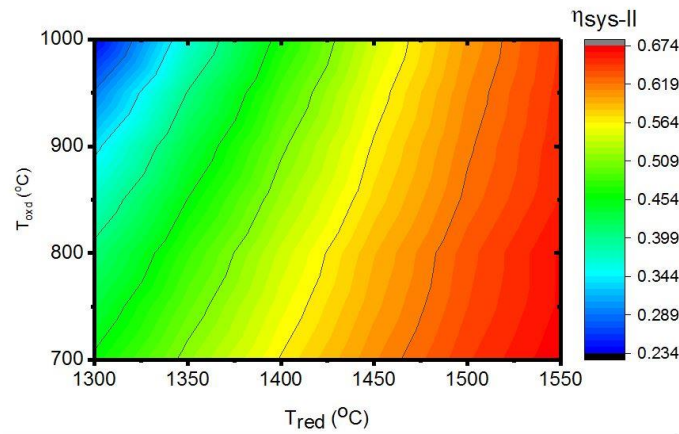

Fig. 6. System efficiency of the ceria for varying temperatures of reduction and oxidation reactors.

It is noted that from figure 6, the efficiency of the system is depended on both the reactor temperatures. With increase of difference of temperature the efficiency of the system increases. With lowest temperature difference between the reactors, the achieved efficiency was 23.4% and with higher the temperature difference, the efficiency of the system increases to 67.4%. For optimal H_2/CO ratio, the oxidation temperature range was between 800-900°C and reduction reactor between 1400-1500°C is in the range of 50-56% quantitatively.

5. Conclusion

In the paper, we developed an interconnected fluidized bed model for chemical looping of ceria for two step syngas thermochemical dissociation of CO_2 and H_2. The hydrodynamics and kinetics for the model is written and compiled in FORTRAN kinetic subroutine and hooked in Aspen Plus

V8.8. It was considered that both oxidation and reduction reactors were operating in bubbling fluidized regime. It is assumed that the reduction reactor heat is supplied by solar energy heat source that could raise the temperature between 1300-1550°C. The oxidation reactor where the CO_2/H_2O was fed for their splitting was varied between 700-1000°C. The effect of difference temperature between the reactors was investigated and found that for optimal H_2/CO ratio the oxidation temperature has to be between 700-900°C. It is found that the maximum efficiency achieved is 67.4% corresponds to highest temperature difference between the reactors but the optimal condition described would have efficiency of around 56.4%.

References

[1] D. Y. C. Leung, G. Caramanna, and M. M. Maroto-Valer, "An overview of current status of carbon dioxide capture and storage technologies," *Renew. Sustain. Energy Rev.*, vol. 39, pp. 426–443, 2014.

[2] C. Wang, L. Chen, S. Xia, and F. Sun, "Maximum production rate optimization for sulphuric acid decomposition process in tubular plug-flow reactor," *Energy*, vol. 99, pp. 152–158, 2016.

[3] C. Wang, L. Chen, S. Xia, and F. Sun, "Optimal Concentration Configuration of Consecutive Chemical ReactionA ⇔ B ⇔ C for Minimum Entropy Generation," *J. Non-Equilibrium Thermodyn.*, vol. 41, no. 4, pp. 313–326, 2016.

[4] M. Aresta, A. Dibenedetto, and A. Angelini, "The changing paradigm in CO2utilization," *J. CO2 Util.*, vol. 3–4, pp. 65–73, 2013.

[5] C. Agrafiotis, M. Roeb, and C. Sattler, "A review on solar thermal syngas production via redox pair-based water/carbon dioxide splitting thermochemical cycles," *Renew. Sustain. Energy Rev.*, vol. 42, pp. 254–285, 2015.

[6] E. Alonso and M. Romero, "Review of experimental investigation on directly irradiated particles solar reactors," *Renew. Sustain. Energy Rev.*, vol. 41, pp. 53–67, 2015.

[7] S. Lorentzou, G. Karagiannakis, D. Dimitrakis, C. Pagkoura, A. Zygogianni, and A. G. Konstandopoulos, "Thermochemical Redox Cycles over Ce-based Oxides," *Energy Procedia*, vol. 69, pp. 1800–1809, 2015.

[8] D. Yadav and R. Banerjee, "A review of solar thermochemical processes," *Renew. Sustain. Energy Rev.*, vol. 54, pp. 497–532, 2016.

[9] J. R. Scheffe and A. Steinfeld, "Oxygen exchange materials for solar thermochemical splitting of H2O and CO2: A review," *Mater. Today*, vol. 17, no. 7, pp. 341–348, 2014.

[10] A. Steinfeld, "Solar thermochemical production of hydrogen - A review," *Sol. Energy*, vol. 78, no. 5, pp. 603–615, 2005.

[11] P. Furler, J. R. Scheffe, D. Marxer, and A. Steinfeld, "Solar reactors for thermochemical CO 2 and H 2 O splitting via metal oxide redox reactions," 2014.

[12] U. W. Hartley, N. Ngoenthong, K. Cheenkachorn, and T. Sornchamni, "CO 2 to Syngas : Metal Oxides on Stainless Steel 316L for micro- channel reactor application," no. 1, pp. 8–11.

[13] S. Tescari *et al.*, "Thermochemical solar energy storage via redox oxides: Materials and reactor/heat exchanger concepts," *Energy Procedia*, vol. 49, pp. 1034–1043, 2013.

[14] Q. Jiang, Z. Chen, J. Tong, M. Yang, Z. Jiang, and C. Li, "Catalytic Function of IrOxin the Two-Step Thermochemical CO2-Splitting Reaction at High Temperatures," *ACS Catal.*, vol. 6, no. 2, pp. 1172–1180, 2016.

[15] N. Gokon, T. Suda, and T. Kodama, "Oxygen and hydrogen productivities and repeatable reactivity of 30-mol%-Fe-, Co-, Ni-, Mn-doped CeO2-δfor thermochemical two-step water-splitting cycle," *Energy*, vol. 90, pp. 1280–1289, 2015.

[16] F. Liu, "Cerium oxide promoted oxygen carrier development and scale modeling study for chemical looping comustion," 2013.

[17] A. Ambrosini, E. N. Coker, A. Mcdaniel, A. Mark, J. A. Ohlhausen, and J. E. Miller, "Oxide materials for thermochemical CO 2 splitting using concentrated solar energy Vision : Sunshine to Petrol," no. August, 2012.

[18]   P. Furler, J. Scheffe, M. Gorbar, L. Moes, U. Vogt, and A. Steinfeld, "Solar Thermochemical CO 2 Splitting Utilizing a Reticulated Porous Ceria Redox System," *Energy & Fuels*, vol. 26, no. 11, pp. 7051–7059, Nov. 2012.

[19]   I. Ermanoski, N. Siegel, and E. Stechel, *A New Reactor Concept for Efficient Solar-Thermochemical Fuel Production*, vol. 135. 2013.

[20]   C. Y. Wen and Y. H. Yu, "A generalized method for predicting the minimum fluidization velocity," *AIChE J.*, vol. 12, no. 3, pp. 610–612, 1966.

[21]   O. Levenspiel, *Chemical reaction engineering*, vol. 38, no. 11. 1999.

[22]   P. N. Rowe, T. J. Evans, and J. C. Middleton, "Transfer of gas between bubbles and dense phase in a two-dimensional fluidised bed," *Chem. Eng. Sci.*, vol. 26, no. 11, pp. 1943–1948, 1971.

[23]   J. H. Pauls, N. Mahinpey, and E. Mostafavi, "Simulation of air-steam gasification of woody biomass in a bubbling fluidized bed using Aspen Plus: a comprehensive model including pyrolysis, hydrodynamics and tar production.," *Biomass and Bioenergy*, vol. 95, pp. 157–166, 2016.

[24]   A. Suwatthikul, S. Limprachaya, P. Kittisupakorn, and I. M. Mujtaba, "Simulation of steam gasification in a fluidized bed reactor with energy self-sufficient condition," *Energies*, vol. 10, no. 3, pp. 1–15, 2017.

[25]   C. Y. Wen and L. H. Chen, "Fluidized bed freeboard phenomena: Entrainment and elutriation," *AIChE J.*, vol. 28, no. 1, pp. 117–128, 1982.

[26]   T. Ishida, N. Gokon, T. Hatamachi, and T. Kodama, "Kinetics of thermal reduction step of thermochemical two-step water splitting using CeO2particles: Master-plot method for analyzing non-isothermal experiments," *Energy Procedia*, vol. 49, pp. 1970–1979, 2013.

[27]   D. Arifin, "Study of redox reactions to split water and carbon dioxide," University of Colorado, 2013.

[28]   F. Taghipour, N. Ellis, and C. Wong, "Experimental and computational study of gas-solid fluidized bed hydrodynamics," *Chem. Eng. Sci.*, vol. 60, no. 24, pp. 6857–6867, 2005.